frontiers | Frontiers in Astronomy and Space Sciences

TYPE Original Research
PUBLISHED 21 September 2023
DOI 10.3389/fspas.2023.1229022

OPEN ACCESS

EDITED BY
Cyprien Verseux,
University of Bremen, Germany

REVIEWED BY
Thierry Dufour,
Université Paris-Sorbonne, France
Adriana Blachowicz,
NASA Jet Propulsion Laboratory (JPL), United States

*CORRESPONDENCE
Laurence Lemelle,
laurence.lemelle@ens-lyon.fr
Christophe Place,
christophe.place@ens-lyon.fr

RECEIVED 25 May 2023
ACCEPTED 01 September 2023
PUBLISHED 21 September 2023

CITATION
Lemelle L, Mottin E, Le Tourneau D, Rouquette S, Campagnolo L, Thévenot C, Maillet A, Barde S, Garre E, Teisseire J, Fontelaye C, Jousseaume V, Pudda C, Constantin O, Marcoux P, Nonglaton G and Place C (2023), Surface contamination rates at different spatial scales in the Columbus module (ISS) during the MATISS campaigns. *Front. Astron. Space Sci.* 10:1229022. doi: 10.3389/fspas.2023.1229022

Surface contamination rates at different spatial scales in the Columbus module (ISS) during the MATISS campaigns

Laurence Lemelle[1]*, Eléonore Mottin[1], Denis Le Tourneau[2], Sébastien Rouquette[3], Lucie Campagnolo[4], Cécile Thévenot[4], Alain Maillet[4], Sébastien Barde[3], Emmanuel Garre[5], Jérémie Teisseire[5], Caroline Fontelaye[6], Vincent Jousseaume[6], Catherine Pudda[6], Olivier Constantin[6], Pierre Marcoux[6], Guillaume Nonglaton[6] and Christophe Place[2]*

[1]University Lyon, ENS de Lyon, University Claude Bernard, CNRS, Laboratoire de Géologie de Lyon-Terre Planètes et Environnement, Lyon, France, [2]University Lyon, ENS de Lyon, CNRS, Laboratoire de Physique, Lyon, France, [3]CNES, Paris, France, [4]MEDES-IMPS for CADMOS, Toulouse, France, [5]Surface du Verre et Interface, UMR CNRS/Saint-Gobain, Aubervilliers, France, [6]Univ. Grenoble Alpes, CEA, LETI, Grenoble, France

Future long-duration human spaceflights require developments to limit biocontamination of surface habitats. The three MATISS (Microbial Aerosol Tethering on Innovative Surfaces in the International Space Station) campaigns exposed surface treatments over several months in the ISS. To this end, eight sample holders designed were mounted with lamella-bearing FDTS ((1*H*, 1*H*, 2*H*, 2*H*)-perfluorodecyltrichlorosilane), SiOCH, and parylene hydrophobic coatings, at two different locations, for several months, during three distinct periods from 2016 to 2020. Tile scanning optical microscopy (×3 and ×30 magnifications) detected several thousand particles, indicating a relatively clean environment (a few particles per mm^2). In previous studies, exposure rates were analyzed for all the coarse and fine particles detected on the largest total area of the integrated FDTS area exposed in the ISS (several cm^2). Here, the contamination rates observed for a smaller constant area unit (the 0.66-cm^2 window area of the holder) were statistically analyzed. Therefore, a statistical difference in rate distributions between RGSH (Return Grid Sensor House) and EDR (European Drawer Rack) and between FDTS and either SiOCH or parylene was shown for the coarse particles but not for the fine particles. The contamination rates were found to be low, confirming the efficiency of the long-term air purification system. The rates tend to vary with the astronaut occupancy rates. Surfaces of spacecraft for long-duration exploration left unmanned during dormancy periods can be considered safe from biocontamination.

KEYWORDS

life support, biomaterials, space applications, space habitation, earth applications, astrobiology, surface biocontamination

1 Introduction

International space agencies are diligently striving to enhance manned spaceflight capabilities for prolonged durations, encompassing missions to diverse destinations, including low Earth orbit (LEO), cis-lunar space, the lunar surface, and ultimately Mars (James et al., 2007; Ott and Pierson, 2014; ISECG, 2018; Salmela et al., 2020). However, the potential biocontamination of enclosed habitats by the microflora carried by the crew presents a significant and unavoidable concern (Yamaguchi et al., 2014; Santomartino et al., 2020). The extended periods of isolation and dependence on closed-loop life support systems (Baranov et al., 2006) in manned stations further amplify this risk. The presence of biocontamination in the cabin not only poses threats to the health of astronauts but also entails potential damage to critical equipment (Ichijo et al., 2016; Farkas and Farkas, 2021). Over time, microorganisms have the capacity to develop resistance, mutate, and increase their virulence, thus transforming benign microbes into pathogenic agents due to the immune system disruptions experienced in space (Jorgensen et al., 1997; Wilson et al., 2007; Wilson et al., 2008; Tirumalai et al., 2017; Zea et al., 2017; Huang et al., 2018; Mukhopadhyay and Bagh, 2020; Fajardo-Cavazos and Nicholson, 2021). Consequently, it is imperative to effectively mitigate these risks (Siegel et al., 2007).

The transmission of pathogens through the air and water present on spacecraft is a critical concern (Novikova, 2004; Novikova et al., 2006; Ichijo et al., 2013; Lang et al., 2017; Acres et al., 2021). To ensure safety, filtration systems play a vital role in purifying these elements and undergo regular monitoring (Ott et al., 2004; Smirnov et al., 2004; Balistreri et al., 2013). Surfaces within the spacecraft harbor a diverse range of microorganisms that can act as sources of infection and contribute to pathogen transmission (Otter et al., 2011; Weber et al., 2013; Otter et al., 2016; Zea et al., 2018; Vaishampayan and Grohmann, 2019; Zea et al., 2020). The formation of biofilms on solid surfaces gives rise to a resilient microbial community capable of withstanding changes in the environment and the effects of antimicrobial agents (Pierson, 2001; Buchovec et al., 2020). As a result, biofilms are strongly associated with the persistence of chronic bacterial infections in humans.

Manual disinfection of surfaces on the International Space Station (ISS) poses challenges for astronauts, particularly when dealing with hard-to-reach areas, due to its labor-intensive and time-consuming nature. Furthermore, in long-duration exploration scenarios where spacecraft may remain unoccupied and unsterilized during dormant periods, the necessity for autonomous microbial monitoring and control systems becomes evident (Sethi and Manik, 2018; Ichijo et al., 2020; Mahnert et al., 2021). Implementing new solutions during the design phase of space modules has proven effective in mitigating the risks of surface biocontamination. Therefore, it is of utmost importance to prioritize the development of durable materials and equipment that limit the microbial growth and prevent its dissemination, thereby ensuring the future success of spacecraft missions (Bauer, 2020; Lin et al., 2020). Selection of materials that are unsuitable for microbial colonization and growth is a promising approach.

There are numerous strategies to limit surface biocontamination, including surfaces that passively repel microorganisms and facilitate their elimination through air purification systems. They constitute a viable option, provided certain constraints are met. These surfaces should be nanoparticle-free, have firmly anchored coatings, should be synthesized using solvent-free automated techniques, and should be compatible with various materials, including glass slides. In microgravity, microorganisms are primarily transported through droplets in non-turbulent laminar flows without thermal convection. Hydrophobic coatings act as a first line of defense by reducing the contact area between the surface and hydrophilic drops, rather than directly reducing adhesion

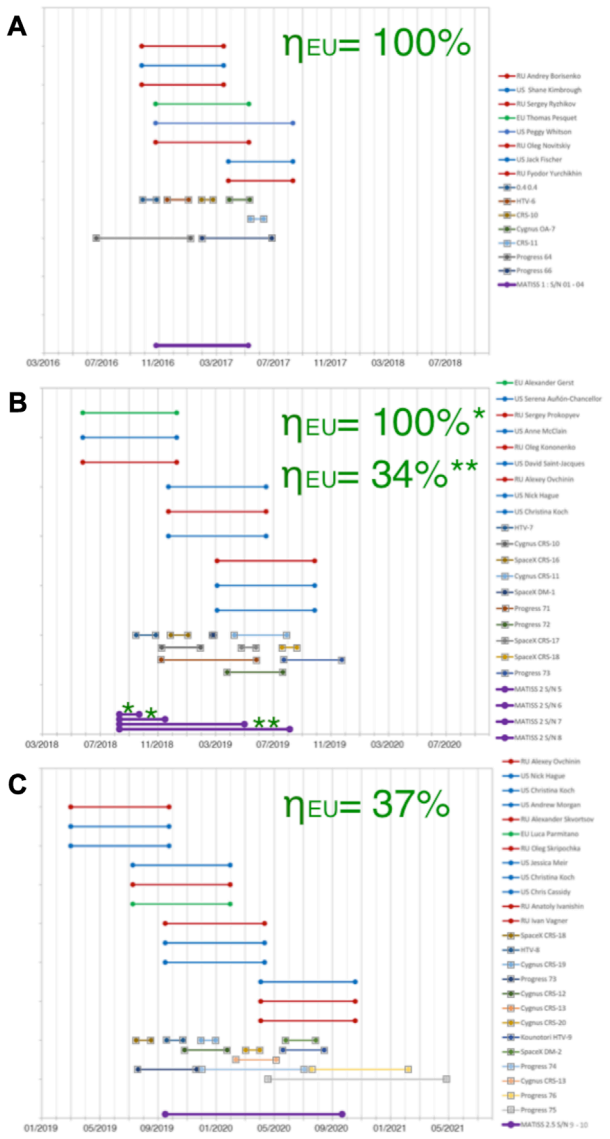

FIGURE 1
Timelines of the MATISS campaigns. **(A)** Dates of MATISS-1. Exposure dates of the holders (bottom, violet). Dates of the visiting vehicles (middle, one color per vehicle, squared tops for line). Dates of each astronaut in the ISS during the campaign (top, blue for the US astronauts, red for the Russian astronauts, and green for the EU astronauts, circled tops for line). The occupancy rate of the EU astronauts ($\sim\eta_{EU}$) during each campaign is reported in green. **(B)** Same for MATISS-2. **(C)** Same for MATISS-2.5.

forces (Glavan et al., 2013; Grinenval et al., 2014; Sadri et al., 2018; Sala de Medeiros et al., 2019). Numerous studies support the effectiveness of hydrophobic coatings in this regard (Moazzam et al., 2016; Chen et al., 2018; Jiang et al., 2020; Kefallinou et al., 2020; Lee et al., 2020; Wang et al., 2020; Li et al., 2021; Mandal et al., 2022).

The MATISS (Microbial Aerosol Tethering on Innovative Surfaces, in the International Space Station) experiment was conducted to explore the application of hydrophobic coatings, commonly used in various industries, for reducing surface biocontamination in spacecraft (Lemelle et al., 2020). In this experiment, surfaces within the Columbus module of the International Space Station were exposed for extended periods using a specially designed holder. This holder ensured the safe exposure of glass surfaces to astronauts and allowed for easy sealing within the station. Upon return to the laboratory, the sealed holder enabled the imaging of particles present on the exposed surfaces. The MATISS experiment was replicated three times between 2016 and 2020, involving the exposure of different surfaces for various durations. For example, the MATISS-1 campaign exposed surfaces for approximately 6 months starting in November 2016, the MATISS-2 campaign involved exposures of approximately 1, 3, and 12 months starting in August 2018, and the MATISS-2.5 campaign lasted for approximately 12 months starting in September 2019 (Figure 1).

In order to limit surface biocontamination, the MATISS experiment was carried out to assess the potential of a particular hydrophobic coating (FDTS) in reducing the biocontamination of surfaces on the ISS (Lemelle et al., 2020; 2022). In these previous studies, we analyzed systematically all the particles that could be detected on the largest area possible and considered them as one set to get average exposure rate values. Here, we analyze more extensively the exposure rates for centimeter-sized sub-unit of surfaces. Sub-sets of rates were newly compiled to evaluate the biocontamination variation between different Columbus positions, different types of hydrophobic coatings, and different time periods. Analyses were performed to display the diversity and variability of the sources and pathways of surface biocontamination observed during extended periods on the ISS.

2 Materials and methods

2.1 Hydrophobic surfaces: coatings and patterning

2.1.1 CEA hydrophobic coatings on silica surfaces

For this study, we selected chemical vapor deposition processes, all carried out in a vacuum on a glass lamella, to limit the use of potentially toxic organic solvents and to provide an excellent intra- and inter-lot reproducibility (Figure 2A).

SiOCH films of 1 µm thickness were deposited using Octamethylcyclotetrasiloxane (OMCTS) as the precursor under vacuum conditions at 2 Torr and 100°C. The water contact angle on SiOCH films was approximately 105 ± 2°. A 1-µm-thick layer of parylene was deposited using the SCS Labcoter® 2 (PDS 2010) Vapor Deposition System with parylene C as the precursor. The

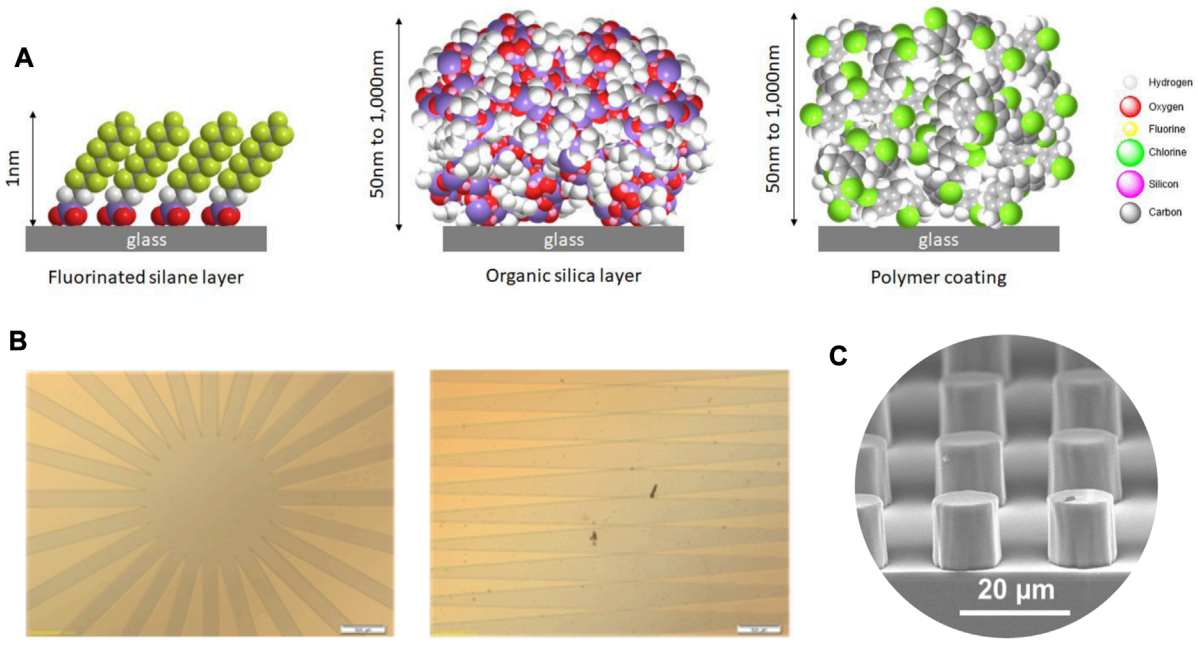

FIGURE 2
Hydrophobic surfaces exposed in the MATISS campaigns. **(A)** Atomic diagram of the molecules constituting the three uniform layers of nanometric thickness and different chemical compositions: fluorinated silane (FDTS, on the left), organic silica (SiOCH, in the middle), and parylene C polymer (on the right). **(B)** Optical images of the masks from which radial and mirror symmetric patterns of FDTS layers have been prepared. **(C)** Patterned layers of micrometric SiO_2 dots.

water contact angle on the parylene layers was approximately 87 ± 4°. The protocols are described in Lemelle et al. (2020).

The process of FDTS coating based on (1*H*, 1*H*, 2*H*, 2*H*)-perfluorodecyltrichlorosilane (FDTS) (ABCR, 97%) was described in Lemelle et al. (2022). The FDTS patterning protocol was as follows: the glass slides were cleaned before they were coated with a positive AZ1512HS photoresist and baked at 100°C. The samples were exposed for 25 s under UV light through a mask with radial and mirror symmetric patterns (Figure 2B). The development of the photoresist was carried out in AZ developer diluted in water under gentle shaking. The hydrophobic FDTS layer was deposited using the MVD100 equipment following the same protocol mentioned previously. Lastly, the rest of the photoresist layer was washed in acetone and ethanol in an ultrasonic bath. The water contact angle on FDTS films was 110 ± 2°.

2.1.2 Saint Gobain superhydrophobic silica surfaces

Pure silica micropatterns at the surface of a silica lamella were fabricated based on the combination of sol–gel process and nanoimprint lithography. The silica pattern was designed during the photolithographic step and functionalized with a vapor-phase deposition of fluorosilane molecules to obtain superhydrophobic surfaces (Dubov et al., 2013). All the characteristic geometrical parameters of the square lattice of circular pillars of the pattern, the height of the pillars (in the range 10 ± 0.5 μm) and the period of grating of 20 mm as well as the pillar diameter, the inter-pillar distance, and the longest dimension evaluated by interference profilometry and SEM (Figure 2C) and the corresponding water contact angle of approximately 135°, were reported in Dubov et al. (2013).

2.2 Holder and dedicated optical microscopy

2.2.1 The MATISS holder

In practice, the MATISS holder (8.5 cm × 6 cm × 1.2 cm, Figure 3A) can be considered a vented aluminum container with a 2-mm-thick slit between a transparent polycarbonate lid and the glass surfaces, allowing a laminar airflow on the surface of the mounted glass lamellae. The transition from the "laboratory-confined" state to the "ISS-exposed" state of the glass surfaces was manually operated by removing Kapton tape that sealed the slit and reversely by repositioning the Kapton tape. The aluminum mounting base has two slots that can be plugged using

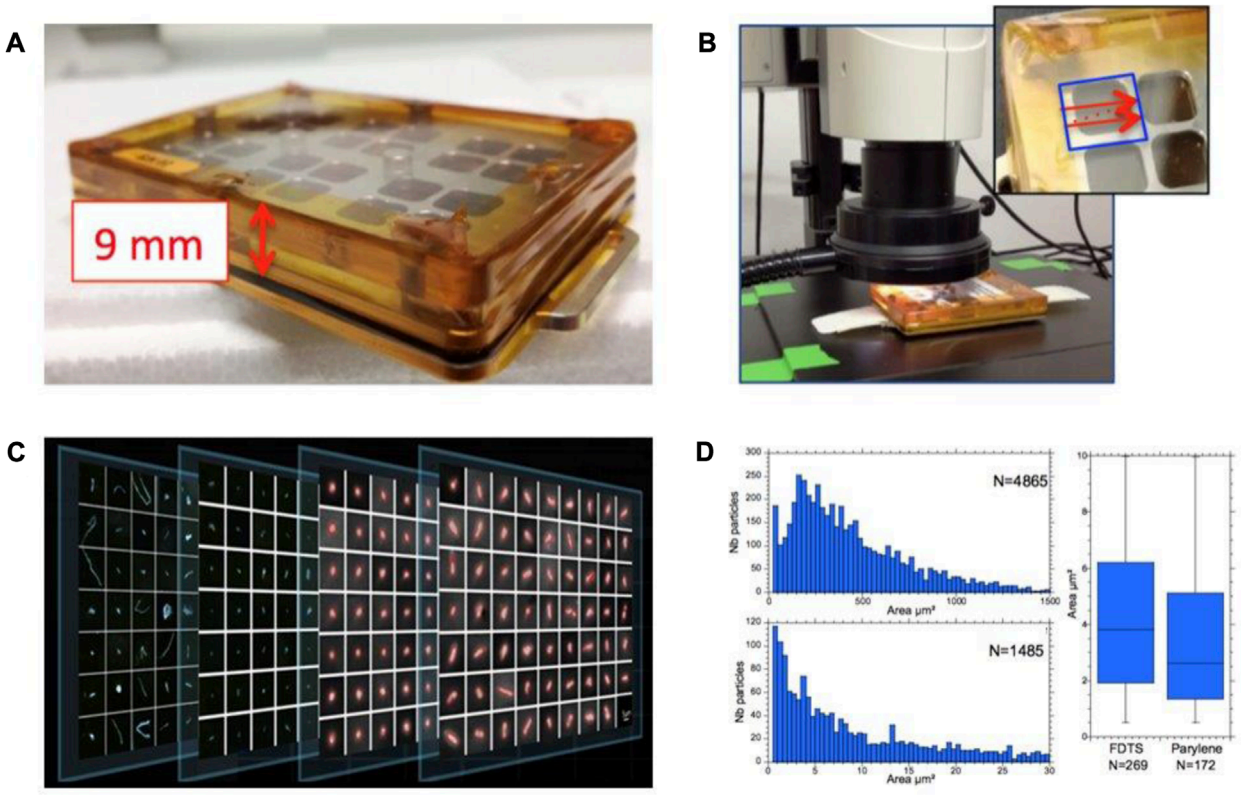

FIGURE 3
Optical microscopy and image analyses. **(A)** MATISS sample holder has lateral openings, here sealed with golden Kapton tape. **(B)** Holder was mounted on a scanning table. All the surface lamellae were imaged across the four windows of the holder (see inset and the blue frame) using a microscope. **(C)** Data treatment of each image at ×3 and ×30 magnifications generated crops for each particle. They are sorted and classified versus their X and Y coordinates and their area in the two sets of coarse (area > 50 μm^2) and fine (area < 50 μm^2) particles. **(D)** Particle size distributions are displayed as histograms, here all the coarse particles of MATISS-1 (top, left) and the fine particles (bottom, left), or as boxplots if the numbers are small (here FDTS and parylene coatings in a holder of MATISS-1).

TABLE 1 Coarse and fine particle rate values (particles.mm^{-2}.month^{-1}) measured on each window from the density (d in particles.mm^{-2}) during the three MATISS campaigns. Exposure location, exposure duration, types of coating [FDTS, SiOCH, and parylene (par.)], and nature of the lamella (glass or quartz) are reported.

Campaign		Location		Lamella		Total exposure time				Coarse particle		Fine particle	
Name	Year	Holder	Position	Support	Coating	Begin	End	N (Days)	N (months)	d	Rate	d	Rate
MATISS-1	2016/2017	H02	RGHS	Glass	FDTS	20/11/16	01/06/17	193	6	1.70	0.26	1.43	0.22
MATISS-1	2016/2017	H02	RGHS	Glass	FDTS	20/11/16	01/06/17	193	6	1.37	0.21	ND	ND
MATISS-1	2016/2017	H02	RGHS	Glass	FDTS	20/11/16	01/06/17	193	6	2.52	0.39	ND	ND
MATISS-1	2016/2017	H02	RGHS	Glass	FDTS	20/11/16	01/06/17	193	6	2.38	0.37	ND	ND
MATISS-1	2016/2017	H03	RGHS	Glass	FDTS	20/11/16	01/06/17	193	6	2.18	0.34	8.35	1.30
MATISS-1	2016/2017	H03	RGHS	Glass	FDTS	20/11/16	01/06/17	193	6	4.48	0.70	ND	ND
MATISS-1	2016/2017	H03	RGHS	Glass	FDTS	20/11/16	01/06/17	193	6	3.08	0.48	ND	ND
MATISS-1	2016/2017	H03	RGHS	Glass	FDTS	20/11/16	01/06/17	193	6	3.23	0.50	ND	ND
MATISS-1	2016/2017	H04	EDR	Glass	FDTS	20/11/16	01/06/17	193	6	1.73	0.27	2.65	0.41
MATISS-1	2016/2017	H04	EDR	Glass	FDTS	20/11/16	01/06/17	193	6	2.05	0.32	5.35	0.83
MATISS-1	2016/2017	H04	EDR	Glass	FDTS	20/11/16	01/06/17	193	6	2.73	0.42	ND	ND
MATISS-1	2016/2017	H04	EDR	Glass	FDTS	20/11/16	01/06/17	193	6	1.97	0.31	ND	ND
MATISS-1	2016/2017	H02	RGHS	Glass	SiOCH	20/11/16	01/06/17	193	6	2.33	0.36	ND	ND
MATISS-1	2016/2017	H02	RGHS	Glass	SiOCH	20/11/16	01/06/17	193	6	1.65	0.26	ND	ND
MATISS-1	2016/2017	H02	RGHS	Glass	SiOCH	20/11/16	01/06/17	193	6	0.75	0.12	ND	ND
MATISS-1	2016/2017	H02	RGHS	Glass	SiOCH	20/11/16	01/06/17	193	6	1.43	0.22	2.18	0.34
MATISS-1	2016/2017	H03	RGHS	Glass	SiOCH	20/11/16	01/06/17	193	6	1.80	0.28	1.07	0.17
MATISS-1	2016/2017	H03	RGHS	Glass	SiOCH	20/11/16	01/06/17	193	6	0.98	0.15	ND	ND
MATISS-1	2016/2017	H03	RGHS	Glass	SiOCH	20/11/16	01/06/17	193	6	0.92	0.14	ND	ND
MATISS-1	2016/2017	H03	RGHS	Glass	SiOCH	20/11/16	01/06/17	193	6	1.85	0.29	ND	ND
MATISS-1	2016/2017	H04	EDR	Glass	SiOCH	20/11/16	01/06/17	193	6	1.42	0.22	4.60	0.72
MATISS-1	2016/2017	H04	EDR	Glass	SiOCH	20/11/16	01/06/17	193	6	1.27	0.20	7.35	1.14
MATISS-1	2016/2017	H04	EDR	Glass	SiOCH	20/11/16	01/06/17	193	6	0.87	0.13	ND	ND
MATISS-1	2016/2017	H04	EDR	Glass	SiOCH	20/11/16	01/06/17	193	6	1.32	0.20	ND	ND
MATISS-1	2016/2017	H02	RGHS	Glass	Par.	20/11/16	01/06/17	193	6	1.42	0.22	ND	ND
MATISS-1	2016/2017	H02	RGHS	Glass	Par.	20/11/16	01/06/17	193	6	1.30	0.20	ND	ND
MATISS-1	2016/2017	H02	RGHS	Glass	Par.	20/11/16	01/06/17	193	6	1.48	0.23	ND	ND
MATISS-1	2016/2017	H02	RGHS	Glass	Par.	20/11/16	01/06/17	193	6	1.28	0.20	3.45	0.54
MATISS-1	2016/2017	H03	RGHS	Glass	Par.	20/11/16	01/06/17	193	6	1.92	0.30	5.98	0.93
MATISS-1	2016/2017	H03	RGHS	Glass	Par.	20/11/16	01/06/17	193	6	2.05	0.32	ND	ND
MATISS-1	2016/2017	H03	RGHS	Glass	Par.	20/11/16	01/06/17	193	6	1.37	0.21	ND	ND
MATISS-1	2016/2017	H03	RGHS	Glass	Par.	20/11/16	01/06/17	193	6	1.48	0.23	ND	ND
MATISS-1	2016/2017	H04	EDR	Glass	Par.	20/11/16	01/06/17	193	6	1.37	0.21	2.37	0.37
MATISS-1	2016/2017	H04	EDR	Glass	Par.	20/11/16	01/06/17	193	6	1.00	0.16	1.67	0.26
MATISS-1	2016/2017	H04	EDR	Glass	Par.	20/11/16	01/06/17	193	6	0.75	0.12	ND	ND
MATISS-1	2016/2017	H04	EDR	Glass	Par.	20/11/16	01/06/17	193	6	0.50	0.08	ND	ND
MATISS-2	2018	H05	RGHS	Glass	FDTS	23/08/18	03/10/18	41	1	0.47	0.34	2.25	1.65
MATISS-2	2018	H05	RGHS	Glass	FDTS	23/08/18	03/10/18	41	1	0.55	0.40	1.72	1.26

(Continued on the following page)

TABLE 1 (*Continued*) **Coarse and fine particle rate values (particles.mm^{-2}.month^{-1}) measured on each window from the density (d in particles.mm^{-2}) during the three MATISS campaigns. Exposure location, exposure duration, types of coating [FDTS, SiOCH, and parylene (par.)], and nature of the lamella (glass or quartz) are reported.**

Campaign		Location		Lamella		Total exposure time				Coarse particle		Fine particle	
Name	Year	Holder	Position	Support	Coating	Begin	End	N (Days)	N (months)	d	Rate	d	Rate
MATISS-2	2018	H05	RGHS	Glass	FDTS	23/08/18	03/10/18	41	1	0.67	0.49	1.82	1.33
MATISS-2	2018	H05	RGHS	Glass	FDTS	23/08/18	03/10/18	41	1	0.63	0.46	1.50	1.10
MATISS-2	2018	H06	RGHS	Glass	FDTS	23/08/18	26/11/18	95	3	0.75	0.24	2.47	0.78
MATISS-2	2018	H06	RGHS	Glass	FDTS	23/08/18	26/11/18	95	3	1.57	0.49	2.13	0.67
MATISS-2	2018	H06	RGHS	Glass	FDTS	23/08/18	26/11/18	95	3	1.48	0.47	6.60	2.08
MATISS-2	2018	H06	RGHS	Glass	FDTS	23/08/18	26/11/18	95	3	1.62	0.51	4.07	1.28
MATISS-2	2018	H08	RGHS	Glass	FDTS	23/08/18	12/08/19	354	12	3.33	0.28	2.05	0.17
MATISS-2	2018	H08	RGHS	Glass	FDTS	23/08/18	12/08/19	354	12	1.13	0.10	2.73	0.23
MATISS-2	2018	H08	RGHS	Glass	FDTS	23/08/18	12/08/19	354	12	2.12	0.18	7.15	0.61
MATISS-2	2018	H08	RGHS	Glass	FDTS	23/08/18	12/08/19	354	12	1.47	0.12	6.78	0.57
MATISS-2.5	2019/2020	H09	RGHS	Glass	FDTS	25/09/19	24/09/20	365	12	0.30	0.02	0.58	0.05
MATISS-2.5	2019/2020	H09	RGHS	Glass	FDTS	25/09/19	24/09/20	365	12	0.33	0.03	0.58	0.05
MATISS-2.5	2019/2020	H09	RGHS	Glass	FDTS	25/09/19	24/09/20	365	12	0.27	0.02	0.47	0.04
MATISS-2.5	2019/2020	H09	RGHS	Glass	FDTS	25/09/19	24/09/20	365	12	0.35	0.03	0.37	0.03
MATISS-2.5	2019/2020	H10	RGHS	Quartz	FDTS	25/09/19	24/09/20	365	12	0.65	0.05	1.62	0.13
MATISS-2.5	2019/2020	H10	RGHS	Quartz	FDTS	25/09/19	24/09/20	365	12	0.42	0.03	2.08	0.17
MATISS-2.5	2019/2020	H10	RGHS	Quartz	FDTS	25/09/19	24/09/20	365	12	0.28	0.02	1.07	0.09
MATISS-2.5	2019/2020	H10	RGHS	Quartz	FDTS	25/09/19	24/09/20	365	12	0.25	0.02	1.37	0.11

Velcro bands. Here, the measurement was sorted by the window area for the particles observed on the circa (8 × 8 mm^2) area (Table 1).

2.2.2 Optical microscopy and image analyses

The MATISS sample holders were placed on an X-Y table for imaging (Figure 3B). A tile scanning mode with a Leica Z16 ApoA MacroFluo optical microscope and a camera setup was used to capture images of the glass surface through the polycarbonate cover. Image processing techniques were applied to identify and measure the position and area of each particle where images were cropped and sorted into different area classes (Figure 3C).

Segmentation and refinement methods were used to analyze the particles in the images. Fine particles have an area < 50 µm^2, and coarse particles have an area > 50 µm^2. These processes were described in Lemelle et al. (2020). The statistic properties could then be studied for different data sets and classically plotted as distributions, for example, the distribution per area for the coarse (Figure 3D left, top) and fine (Figure 3D left, bottom) particles on all coatings of MATISS-1, or boxplots, such as the boxplot of the area of fine particles in a holder on a given coating (Figure 3D right).

In this study, each glass lamella was observed below four windows (8 × 8 mm^2), and the surface density for each window (in particles.mm^{-2}) was determined for both the fine and coarse particles to statistically investigate the surface contamination.

3 Results

Throughout the three MATISS campaigns, the holders were strategically positioned at two different locations within the Columbus module ("RGHS" for "Return Grid Sensor House" and "EDR" for "European Drawer Rack," Figure 4), mounted with different hydrophobic coatings, and exposed during different periods. While the coarse (area > 50 µm^2) and fine (area < 50 µm^2) particles detected on the RGHS location were initially pooled to be investigated. Here we compile and analyze the contamination at a finer grained scale, for the 56 probed windows versus the locations, periods, types of coating (Table 1).

3.1 Exposure at different periods

The MATISS experiments were conducted in triplicate from 2016 to 2020. Surfaces were exposed over several months: ~6 months from November 2016 for the MATISS-1 campaign; ~1, ~3, and ~12 months from August 2018 for the MATISS-2 campaign; and ~12 months from September 2019 for the MATISS-2.5

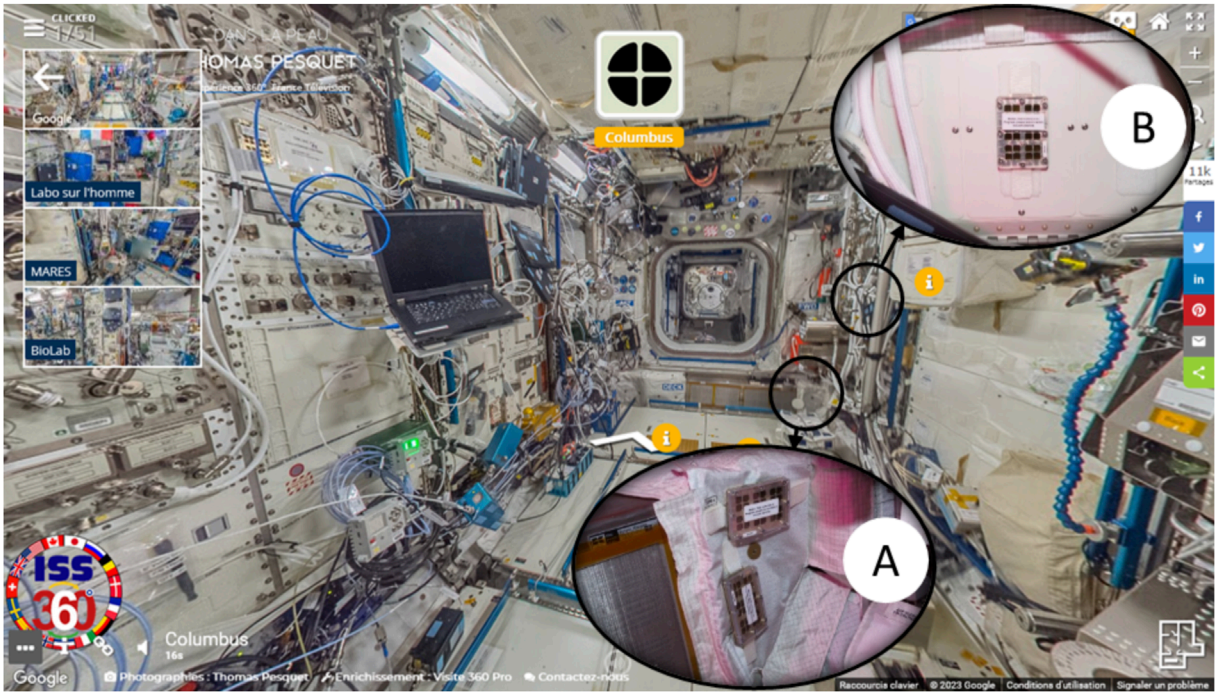

FIGURE 4
Photographs of the sample holders installed in the Columbus module. **(A)** Two holders installed near the Return Grid Sensor Housing (RGHS) and **(B)** one holder installed in front of the European Physiology Module's (EPM facility) front panel on the EDR front panel. Crops are photograph courtesy of NASA/ESA, which are permissible to use within the public domain superimposed on a Google Street View of the Columbus module.

campaign (Figure 1). The three average values of the contamination rates of the FDTS coatings exposed at the RGSH location previously compiled for each of the three MATISS campaigns (from November 2016 to 2020, Figure 1) were shown to be similar in the MATISS-1 and MATISS-2 campaigns whereas notably lower in the MATISS-2.5 campaign for both coarse and fine particles (Lemelle et al., 2022).

Statistical differences between the distributions of the rates compiled per window for all types of coatings, exposure times, and locations in the MATISS-2.5 campaign and the rates in MATISS-1 and 2 campaigns (Table 1; Figure 5A) were examined by unpaired Student's *t*-test. The values remain very significantly different for both the coarse and fine particles (p-values < 10^{-3}). The average rate of coarse particles in the MATISS-1 and MATISS-2 campaigns (0.30 ± 0.09 particles.mm^{-2}.month^{-1} for N = 24) is higher than that in MATISS-2.5 (0.23 ± 0.07 particles.mm^{-2}.month^{-1}, mean ± SD for N = 12). The average rate of fine particles in the MATISS-1 and MATISS-2 campaigns (0.79 ± 0.40 particles.mm^{-2}.month^{-1} for N = 24) is higher than that in MATISS-2.5 (0.08 ± 0.04 particles.mm^{-2}.month^{-1} for N = 8).

3.2 Exposure rates at RGHS and EPM

During the MATISS-1 campaigns, holders were installed simultaneously in two specific locations on the Columbus module for approximately 6 months starting from November 2016 (Figure 1). The first location was in close proximity to the return grid, where the majority of the cabin air in Columbus was extracted at a rate of 400 m^3/h and reintroduced into the adjacent module. Two holders were positioned near the hatch (Figure 4). The crew's activities in this area were limited to manual filter maintenance or cleaning tasks. Throughout the monthly exposure periods, particles were continuously transported by the airflow. The air velocity near the holders was modeled to be 0.21 m/s (approximately 40 ft/min). The second location was situated in front of the EPM (European Physiology Module) rack on the EDR, located in the central section of the Columbus cabin (Figure 4). The primary source of the airflow in this area was an air outlet positioned approximately 1 m above the exposure area. This outlet expelled 55 m^3/h of air, but the flow was directed toward the center of the cabin rather than the surface of the holder.

We examine the contamination rate values in the RGSH and EDR locations after exposure over 6 months during the MATISS-1 campaign (Table 1; Figure 5B). The statistical difference in coarse particle rate distributions between RGSH and EDR was examined by unpaired Student's *t*-test and found to be significantly different (p-values < 0.03) contrary to that of the fine particle rates (p = 0.43). The average rate distribution of coarse particles in the RGSH location (0.30 ± 0.09 particles.mm^{-2}.month^{-1} for N = 24) is higher than that in EDR (0.23 ± 0.07 particles.mm^{-2}.month^{-1}, mean ± SD for N = 12). The average rate distribution of the fine particles (0.63 ± 0.33 particles.mm^{-2}.month^{-1}, mean ± SD for N = 12) is higher than that of the coarse particles.

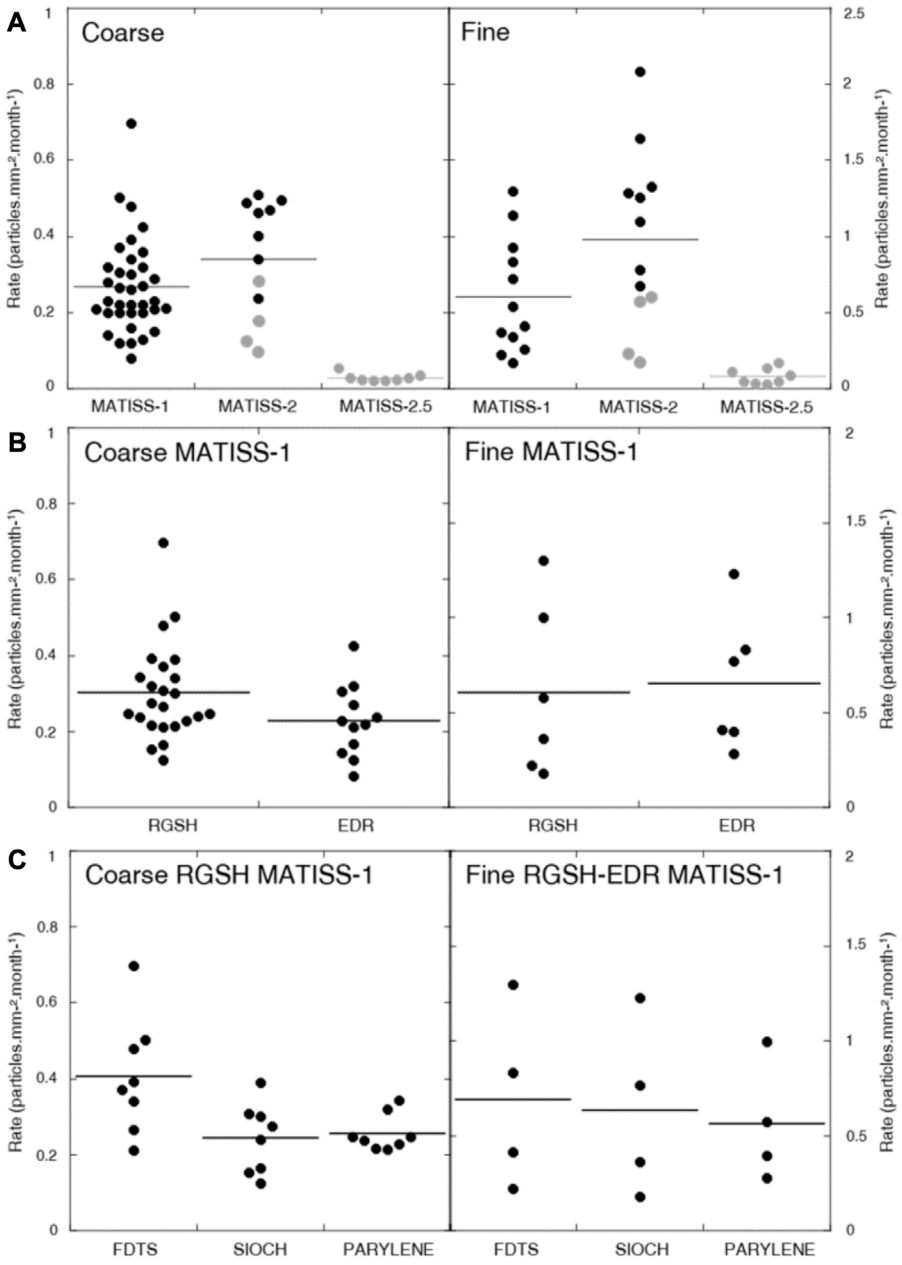

FIGURE 5
Surface contamination rates. **(A)** Coarse particle rates (left) and fine particle rates (right) versus the different MATISS campaigns versus the occupancy rate value (100% in black; approximately 35% in gray). **(B)** Coarse particle rates (left) and fine particle rates (right) in the MATISS-1 campaign versus the different locations. **(C)** Coarse particle rates (left) and fine particle rates (right) in the MATISS-1 campaign and RGSH location versus the different coatings. The mean values are shown as horizontal lines. All data are tabulated in Table 1.

3.3 Exposure rates on different hydrophobic coatings

The biocontamination was, therefore, probed from the MATISS-1 campaigns in the RGHS location versus the three types of hydrophobic coatings (FDTS, SiOCH, and parylene). The contours of the fine particles, observed on the Saint Gobain superhydrophobic surfaces, could not be sorted with the same data treatment. The pillars of the textured surface show brighter contrasts on their edge, impeding and altering a systematic and exhaustive image processing. Therefore, the particle's area and the fine and coarse particle sets herein sorted are difficult to compare to those observed on the hydrophobic coatings. Similarly, the FDTS-patterned surfaces displayed numerous particles, among which coarse particles were identified as default products of the process. For higher hydrophobicity (FDTS > SiOCH > parylene), the coating should favor adhesion of the coarse hydrophobic particles. Conversely, it hinders more the fine particles, that are brought to the surface with their own hydrous sphere or through water droplet deposition.

Given the significant difference in the contamination rates in the RGSH and EDR locations for the coarse particles, these rates were not pooled compared to the fine particles. Statistical differences between the distributions of the rates compiled per window on the FDTS and either on SiOCH or parylene (Table 1; Figure 5C) were examined by unpaired Student's *t*-test. The rates on FDTS are found to be significantly higher for the coarse particles (*p*-values = 0.01), which is less clear for the fine particle rates (p = 0.35). The average rate of coarse particles on FDTS (0.40 ± 0.11 particles.mm^{-2}.month^{-1}, mean ± SD for N = 8) is higher than that on both the SiOCH (0.24 ± 0.03 particles.mm^{-2}.month^{-1}, mean ± SD for N = 8) and parylene (0.25 ± 0.04 particles.mm^{-2}.month^{-1}, mean ± SD for N = 8). The average rate value for the fine particles is 0.63 ± 0.33 particles.mm^{-2}.month^{-1}, mean ± SD for N = 12.

4 Discussion and conclusion

The significant difference among the tested distributions of rates is particularly evident when comparing the various campaigns. As previously proposed, these rates can be presented in regard of the two range values of the occupancy rates of the Columbus module for each campaign, η_{EU} (%). The occupancy rate is estimated as the fraction of time an EU astronaut (green line in Figure 1) is present in the ISS during the holder's exposure (violet line in Figure 1). Values reported in Figure 1 were evaluated considering only the occupancy periods of the European astronauts who are the module's main occupants. The values were found to be 100% for MATISS-1 and some of the holders of MATISS-2 and approximately 35% for MATISS-2.5 and one holder of MATISS-2 (Lemelle et al., 2022). These findings support the conclusion drawn for the sets of all the particles of each campaign, suggesting that contamination rate differences are associated with ISS activity, likely influenced by astronaut occupancy (Lemelle et al., 2022). During periods of high occupancy in MATISS-1 and MATISS-2 (in black in Figure 5A), there is a noticeable increase in coarse and fine particle contamination levels. In contrast, when the occupancy is low (approximately 35%, in gray in Figure 5A), contamination remains relatively low in both MATISS-2 and MATISS-2.5. To some extent, the rates appear to be lower in MATISS-2.5, which may be correlated with an even lower activity of the astronauts during the COVID period. MATISS-2.5 may be close to the lower contamination rates that can be detected with our experimental setup.

Occupancy integrates multi-parameters from various sources and routes of surface contamination by fine and coarse particles over long periods of exposure. During these periods, both the sources and modes of contamination can change and evolve. In long-duration space missions, the astronaut microbiome evolves (Voorhies et al., 2019), and these changes differ among the crew members (Morrison et al., 2021). Despite the dynamic nature of the individual crew members' microbiome composition and diversity, a delayed process of microbial homogenization between the crew and habitat surfaces is expected (Mahnert et al., 2021). The crew's microbiome effectively contaminates abiotic surfaces in a confined cabin. The specific pathways of contamination, like through aerosols or shed skin fragments, and the amount of contamination can vary based on the number of astronauts, types, and intensity of activities carried out by the crew members.

The tested distributions show a difference near the RGSH and EDR positions regarding coarse particles. No such distinction is observed for fine particles despite contamination rates being twice higher. The surface contamination by the coarse particles, even if cumulated over more than 6 months, is not averaged at the scale of the Columbus modulus. The involvement of astronauts in activities near RGSH and EDR likely contributes to the local contamination by the coarse particles, and this factor should not be underestimated. Conversely, surface contamination by fine particles is spatially uniform, emphasizing that coatings are relevant at the first order to limit the rate of fine particle contamination. For fine particles, a noticeable property of rate distribution is the much higher relative error value (~50%) than the coarse particle rates (~30%). This may be interpreted by a spatial homogeneity higher for the coarse than the fine particles at the scale of the holders, likely displaying different advection and deposition modes.

A difference between the rates of FDTS and other coatings among the tested distributions is only observed for coarse particles and is somewhat uncertain, primarily due to over-sampling. Additional investigations such as the fraction of thinner particles (Lemelle et al., 2020), kinetics, or spatial distribution analysis at the window scale are needed to determine the potential benefits of hydrophobic coatings in reducing biocontamination on surfaces within the ISS (Lemelle et al., 2022). The substantial relative error for each coating type indicates a high level of heterogeneity at the holder and possibly lamella scales, suggesting the presence of a surface depot resulting from an irregular and heterogeneous aerosol pathway.

In this study, the comprehensive analysis conducted at a fine-grain scale offers an approach to investigate the sources and pathways of contamination in the Columbus module over extended periods. The findings confirm that, regardless of the parameters considered, the contamination rate per window area is low, indicating the effectiveness of the long-term air purification system. Moreover, it is observed that higher contamination rates occur during periods when astronaut occupancy increases. Although there may be temporary variations linked to specific activities, especially for coarse particles, this trend suggests that surface contamination over periods exceeding 6 months can be approximated by a constant rate directly proportional to the number of astronauts present. Consequently, unmanned spacecraft during dormant periods, as expected in long-duration exploration, are likely to exhibit significantly lower levels of surface contamination (Ott, 2016; LaPelusa et al., 2021; Bijlani et al., 2021).

Data availability statement

The original contributions presented in the study are included in the article; further inquiries can be directed to the corresponding authors.

Author contributions

LL, CP, LC, AM, and SB designed the MATISS-1 project; LL, CP, and SR designed the MATISS-2 project; LL, CP, GN, and SR designed the MATISS-2.5 project; DL and EM machined the sample holder

and carried out the microscopy imaging; GN, CF, VJ, CaP, OC, JT, and EG prepared the surfaces; PM carried out the microbiological investigations; LC, CT, AM, and SB managed the qualification for spaceflight of the MATISS-1 experiment and the communication with the astronauts; CT and SR managed the qualification for spaceflight of the MATISS-2 and MATISS-2.5 experiments and the communication with the astronauts; LL, CP, and GN wrote the paper. All authors contributed to the article and approved the submitted version.

Funding

The CNES, the French space agency, provided financial support for the MATISS hardware design and for the MATISS experiments.

Acknowledgments

The authors thank the NASA and ESA astronauts that were involved in the MATISS experiments. The authors also acknowledge the contribution of SFR BioSciences (UMS3444/CNRS, US8/Inserm, ENS de Lyon, UCBL) PLATIM facility. CEA-Leti acknowledges the support of the Agence Nationale de la Recherche through the LabEx ARCANE program (ANR-11-LABX-0003-01) and the Graduate School on Chemistry, Biology and Health of Université Grenoble Alpes CBH-EUR-GS (ANR-17-EURE-0003). Anne-Dominique Malinge and Philippe Boulez contributed to the final integration of the MATISS experiments.

Conflict of interest

The authors declare that the research was conducted in the absence of any commercial or financial relationships that could be construed as a potential conflict of interest.

Publisher's note

References

Acres, J. M., Youngapelian, M. J., and Nadeau, J. (2021). The influence of spaceflight and simulated microgravity on bacterial motility and chemotaxis. *npj Microgravity* 7, 7–11. doi:10.1038/s41526-021-00135-x

Balistreri, S. F., Steele, J. W., Caron, M. E., and Laliberte, Y. J. (2013). International space station common cabin air assembly condensing heat exchanger hydrophilic coating operation, recovery, and lessons learned. NASA Technical Report JSC-CN-27469. Available at: https://ntrs.nasa.gov/archive/nasa/casi.ntrs.nasa.gov/20130000766.pdf.

Baranov, V. M., Polikarpov, N. A., Novikova, N. D., Deshevaia, E. A., Poddubko, S. V., Svistunova, I., et al. (2006). Main results of the biorisk experiment on the international space station. *Aviakosm. Ekol. Med.* 40 (3–9), 3–9. PMID: 17193961.

Bauer, J. (2020). Microgravity and cell adherence. *Int. J. Mol. Sci.* 21, 2214. doi:10.3390/ijms21062214

Bijlani, S., Stephens, E., Singh, N. K., Venkateswaran, K., and Wang, C. C. C. (2021). Advances in space microbiology. *iScience* 24, 102395. doi:10.1016/j.isci.2021.102395

Buchovec, I., Gricajeva, A., Kalėdienė, L., and Vitta, P. (2020). Antimicrobial photoinactivation approach based on natural agents for control of bacteria biofilms in spacecraft. *Int. J. Mol. Sci.* 21, 6932. doi:10.3390/ijms21186932

Chen, Y., Lu, W., Guo, Y., Zhu, Y., Lu, H., and Wu, Y. (2018). Superhydrophobic coatings on gelatin-based films: fabrication, characterization and cytotoxicity studies. *RSC Adv.* 8, 23712–23719. doi:10.1039/C8RA04066D

Dubov, A. L., Perez-Toralla, K., Letailleur, A., Barthel, E., and Teisseire, J. (2013). Superhydrophobic silica surfaces: fabrication and stability. *J. Micromech. Microeng.* 23, 125013. doi:10.1088/0960-1317/23/12/125013

Fajardo-Cavazos, P., and Nicholson, W. L. (2021). Mechanotransduction in prokaryotes: A possible mechanism of spaceflight adaptation. *Life* 11, 33. doi:10.3390/life11010033

Farkas, Á., and Farkas, G. (2021). Effects of spaceflight on human skin. *Ski. Pharmacol. Physiol.* 34, 239–245. doi:10.1159/000515963

Glavan, A. C., Martinez, R. V., Maxwell, E. J., Subramaniam, A. B., Nunes, R. M. D., Soh, S., et al. (2013). Rapid fabrication of pressure-driven open-channel microfluidic devices in omniphobic RF paper. *Lab. Chip* 13, 2922–2930. doi:10.1039/C3LC50371B

Grinenval, E., Nonglaton, G., and Vinet, F. (2014). Spatially controlled immobilisation of biomolecules: A complete approach in green chemistry. *Appl. Surf. Sci.* 289, 571–580. doi:10.1016/j.apsusc.2013.11.046

Huang, B., Li, D. G., Huang, Y., and Liu, C. T. (2018). Effects of spaceflight and simulated microgravity on microbial growth and secondary metabolism. *Mil. Med. Res.* 5, 18. doi:10.1186/s40779-018-0162-9

Ichijo, T., Yamaguchi, N., Tanigaki, F., Shirakawa, M., and Nasu, M. (2016). Four-year bacterial monitoring in the international space station-Japanese experiment module "kibo" with culture-independent approach. *npj Microgravity* 2, 16007. doi:10.1038/npjmgrav.2016.7

Ichijo, T., Hieda, H., Ishihara, R., Yamaguchi, N., and Nasu, M. (2013). Bacterial monitoring with adhesive sheet in the international space station-"Kibo", the Japanese experiment module. *Microbes Environ.* 28, 264–268. doi:10.1264/jsme2.me12184

Ichijo, T., Shimazu, T., and Nasu, M. (2020). Microbial monitoring in the international space station and its application on earth. *Bio. Pharm. Bul.* 43, 254–257. doi:10.1248/bpb.b19-00912

International Space Exploration Coordination Group (2018). The global exploration roadmap. ISECG Technical Report. Available at: https://www.globalspaceexploration.org/wordpress/wp-content/isecg/GER_2018_small_mobile.pdf.

James, J. T., Parmet, A. J., and Pierson, D. L. (2007). Aerospace toxicology and microbiology. Available at: https://ntrs.nasa.gov/citations/20070032022.

Jiang, R., Hao, L., Song, L., Tian, L., Fan, Y., Zhao, J., et al. (2020). Lotus-leaf-inspired hierarchical structured surface with non-fouling and mechanical bactericidal performances. *Chem. Eng. J.* 398, 125609. doi:10.1016/j.cej.2020.125609

Jorgensen, J. H., Skweres, J. A., Mishra, S. K., McElmeel, M. L., Maher, L. A., Mulder, R., et al. (1997). Development of an antimicrobial susceptibility testing method suitable for performance during space flight. *J. Clin. Microbiol.* 35, 2093–2097. doi:10.1128/jcm.35.8.2093-2097.1997

Kefallinou, D., Ellinas, K., Speliotis, T., Stamatakis, K., Gogolides, E., and Tserepi, A. (2020). Optimization of antibacterial properties of "hybrid" metal-sputtered superhydrophobic surfaces. *Coatings* 10, 25. doi:10.3390/coatings10010025

Lang, J. M., Coil, D. A., Neches, R. Y., Brown, W. E., Cavalier, D., Severance, M., et al. (2017). A microbial survey of the international space station (ISS). *PeerJ* 5, e4029. doi:10.7717/peerj.4029

LaPelusa, M., Donoviel, D., Branzini, S. E., Carlson, P. E., Culler, S., Cheema, A. K., et al. (2021). Microbiome for mars: surveying microbiome connections to healthcare with implications for long-duration human spaceflight, virtual workshop july 13 2020. *Microbiome* 9, 2. doi:10.1186/s40168-020-00951-5

Lee, Y., Chung, Y. W., Park, J., Park, K., Seo, Y., Hong, S. N., et al. (2020). Lubricant-infused directly engraved nano-microstructures for mechanically durable endoscope lens with anti-biofouling and anti-fogging properties. *Sci. Rep.* 10, 17454. doi:10.1038/s41598-020-74517-8

Lemelle, L., Campagnolo, L., Mottin, E., Le Tourneau, D., Garre, E., Marcoux, P., et al. (2020). Towards a passive limitation of particle surface contamination in the Columbus module (ISS) during the MATISS experiment of the Proxima Mission. *npj Microgravity* 6, 29–37. doi:10.1038/s41526-020-00120-w

Lemelle, L., Rouquette, S., Mottin, E., Le Tourneau, D., Marcoux, P. R., Thévenot, C., et al. (2022). Passive limitation of surface contamination by perFluoroDecylTrichloroSilane coatings in the ISS during the MATISS experiments. *npj Microgravity* 8, 31–38. doi:10.1038/s41526-022-00218-3

Li, J., Yuan, T., Zhou, C., Chen, B., Shuai, Y., Wu, D., et al. (2021). Facile Li-Al layered double hydroxide films on Al alloy for enhanced hydrophobicity, anti-biofouling and anti-corrosion performance. *J. Mater. Sci. Technol.* 79, 230–242. doi:10.1016/j.jmst.2020.10.072

Lin, X., Zhang, K., Wei, D., Tian, Y., Gao, Y., Chen, Z., et al. (2020). The impact of spaceflight and simulated microgravity on cell adhesion. *Int. J. Mol. Sci.* 21, 3031. doi:10.3390/ijms21093031

Mahnert, A., Verseux, C., Schwendner, P., Koskinen, K., Kumpitsch, C., Blohs, M., et al. (2021). Microbiome dynamics during the HI-SEAS IV mission, and implications for future crewed missions beyond Earth. *Microbiome* 9, 27. doi:10.1186/s40168-020-00959-x

Mandal, P., Ivvala, J., Arora, H. S., Ghosh, S. K., and Grewal, H. S. (2022). Bioinspired micro/nano structured aluminum with multifaceted applications. *Colloids Surf. B Biointerfaces* 211, 112311. doi:10.1016/j.colsurfb.2021.112311

Moazzam, P., Razmjou, A., Golabi, M., Shokri, D., and Landarani-Isfahani, A. (2016). Investigating the BSA protein adsorption and bacterial adhesion of Al-alloy surfaces after creating a hierarchical (micro/nano) superhydrophobic structure. *J. Biomed. Mater. Res.* 104, 2220–2233. doi:10.1002/jbm.a.35751

Morrison, M. D., Thissen, J. B., Karouia, F., Mehta, S., Urbaniak, C., Venkateswaran, K., et al. (2021). Investigation of spaceflight induced changes to astronaut microbiomes. *Front. Microbiol.* 12, 659179. doi:10.3389/fmicb.2021.659179

Mukhopadhyay, S., and Bagh, S. (2020). A microgravity responsive synthetic genetic device in Escherichia coli. *Biosens. Bioelectron.* 167, 112462. doi:10.1016/j.bios.2020.112462

Novikova, N., De Boever, P., Poddubko, S., Deshevaya, E., Polikarpov, N., Rakova, N., et al. (2006). Survey of environmental biocontamination on board the international space station. *Res. Microbiol.* 157, 5–12. doi:10.1016/j.resmic.2005.07.010

Novikova, N. D. (2004). Review of the knowledge of microbial contamination of the Russian manned spacecraft. *Microb. Ecol.* 47, 127–132. doi:10.1007/s00248-003-1055-2

Ott, C. M., Bruce, R. J., and Pierson, D. L. (2004). Microbial characterization of free floating condensate aboard the Mir Space Station. *Microb. Ecol.* 47, 133–136. doi:10.1007/s00248-003-1038-3

Ott, C. M., Pierson, D. L., Shirakawa, M., Tanigaki, F., Hida, M., Yamazaki, T., et al. (2014). Space habitation and microbiology: status and roadmap of space agencies. *Microb. Environ.* 29, 239–242. doi:10.1264/jsme2.ME2903rh

Ott, C. M. (2016). Risk of adverse health effects due to host-microorganism interactions. Available at: https://ntrs.nasa.gov/search.jsp?R=20170001973.

Otter, J. A., Donskey, C., Yezli, S., Douthwaite, S., Goldenberg, S. D., and Weber, D. J. (2016). Transmission of sars and mers coronaviruses and influenza virus in healthcare settings: the possible role of dry surface contamination. *J. Hosp. Infect.* 92, 235–250. doi:10.1016/j.jhin.2015.08.027

Otter, J. A., Yezli, S., and French, G. L. (2011). The role played by contaminated surfaces in the transmission of nosocomial pathogens. *Infect. Control. Hosp. Epidemiol.* 32, 687–699. doi:10.1086/660363

Pierson, D. L. (2001). Microbial contamination of spacecraft. *Space Biol. Bull.* 14, 1–6. Available at: https://ntrs.nasa.gov/citations/20100036603.

Sadri, B., Goswami, D., Sala de Medeiros, M., Pal, A., Castro, B., Kuang, S., et al. (2018). Wearable and implantable epidermal paper-based electronics. *ACS Appl. Mater. Interfaces* 10, 31061–31068. doi:10.1021/acsami.8b11020

Sala de Medeiros, M., Chanci, D., Moreno, C., Goswami, D., and Martinez, R. V. (2019). Waterproof, breathable, and antibacterial self-powered e-textiles based on omniphobic triboelectric nanogenerators. *Adv. Funct. Mater.* 29, 1904350. doi:10.1002/adfm.201904350

Salmela, A., Kulmala, I., Karvinen, A., Taillebot, V., Weiss, P., Gobert, T., et al. (2020). Measurement and simulation of biocontamination in an enclosed habitat. *Aerosol. Sci. Eng.* 4, 101–110. doi:10.1007/s41810-020-00057-3

Santomartino, R., Waajen, A. C., de Wit, W., Nicholson, N., Parmitano, L., Loudon, C. M., et al. (2020). No effect of microgravity and simulated mars gravity on final bacterial cell concentrations on the international space station: applications to space bioproduction. *Front. Microbiol.* 11, 579156. doi:10.3389/fmicb.2020.579156

Sethi, S. K., and Manik, G. (2018). Recent progress in super hydrophobic/hydrophilic self-cleaning surfaces for various industrial applications: A review. *Polym. Plast. Technol. Eng.* 57, 1932–1952. doi:10.1080/03602559.2018.1447128

Siegel, J. D., Rhinehart, E., Jackson, M., and Chiarello, L. (2007). Guideline for isolation precautions: preventing transmission of infectious agents in health care settings. *Am. J. Infect. Control* 35, S65–S164. doi:10.1016/j.ajic.2007.10.007

Smirnov, E. M., Ivanov, N. G., Telnov, D. S., Son, C. H., and Aksamentov, V. K. (2004). Computational fluid dynamics study of air flow characteristics in the columbus module, *SAE Technical Paper* 01–2500. doi:10.4271/2004-01-2500

Tirumalai, M. R., Karouia, F., Tran, Q., Stepanov, V. G., Bruce, R. J., Ott, C. M., et al. (2017). The adaptation of escherichia coli cells grown in simulated microgravity for an extended period is both phenotypic and genomic. *npj Microgravity* 3, 15–19. doi:10.1038/s41526-017-0020-1

Vaishampayan, A., and Grohmann, E. (2019). Multi-resistant biofilm-forming pathogens on the international space station. *J. Biosci.* 44, 125. doi:10.1007/s12038-019-9929-8

Voorhies, A. A., Mark Ott, C., Mehta, S., Pierson, D. L., Crucian, B. E., Feiveson, A., et al. (2019). Study of the impact of long-duration space missions at the International Space Station on the astronaut microbiome. *Sci. Rep.* 9, 9911. doi:10.1038/s41598-019-46303-8

Wang, T., Huang, L., Liu, Y., Li, X., Liu, C., Handschuh-Wang, S., et al. (2020). Robust biomimetic hierarchical diamond architecture with a self-cleaning, antibacterial, and antibiofouling surface. *ACS Appl. Mater. Interfaces* 12, 24432–24441. doi:10.1021/acsami.0c02460

Weber, D., Anderson, D., and Rutala, W. (2013). The role of the surface environment in healthcare-associated infections. *Curr. Opin. Infect. Dis.* 26, 338–344. doi:10.1097/QCO.0b013e3283630f04

Wilson, J. W., Ott, C. M., Bentrup, K. H., Ramamurthy, R., Quick, L., Porwollik, S., et al. (2007). Space flight alters bacterial gene expression and virulence and reveals a role for global regulator Hfq. *Proc. Nat. Acad. Sci.* 104, 16299–16304. doi:10.1073/pnas.0707155104

Wilson, J. W., Ott, C. M., Quick, L., Davis, R., Bentrup, K. H., Crabbé, A., et al. (2008). Media ion composition controls regulatory and virulence response of Salmonella in spaceflight. *PLoS One* 3, e3923. doi:10.1371/journal.pone.0003923

Yamaguchi, N., Roberts, M., Castro, S., Oubre, C., Makimura, K., Leys, N., et al. (2014). Microbial monitoring of crewed habitats in space—current status and future perspectives. *Microbes Environ.* 29, 250–260. doi:10.1264/jsme2.ME14031

Zea, L., Larsen, M., Estante, F., Qvortrup, K., Moeller, R., Dias de Oliveira, S., et al. (2017). Phenotypic changes exhibited by *E. coli* cultured in space. *Front. Microbiol.* 8, 1598. doi:10.3389/fmicb.2017.01598

Zea, L., McLean, R. J. C., Rook, T. A., Angle, G., Carter, D. L., Delegard, A., et al. (2020). Potential biofilm control strategies for extended spaceflight missions. *Biofilm* 2, 100026. doi:10.1016/j.bioflm.2020.100026

Zea, L., Nisar, Z., Rubin, P., Cortesão, M., Luo, J., McBride, S. A., et al. (2018). Design of a spaceflight biofilm experiment. *Acta Astronaut.* 148, 294–300. doi:10.1016/j.actaastro.2018.04.039